MAGNETOTRANSPORT IN THIN COBALT FILMS FOR SPINTRONICS APPLICATIONS

Department of Physics and Astronomy

The University of Manchester

Semester 2 MPhys report

April 2018

Ben Snow

9630490

Abstract

With the discovery of Graphene came the rapid research into the field of nanometer scale spintronics. Hexagonal boron nitride (hBN) has been used to exploit and enhance the properties of Graphene and ferromagnetic materials, like cobalt, have been used to inject and detect spins into the 2D structure. Building on previous work, a nanodevice was fabricated to measure the resistivity, AMR, thermopower and MTEP of cobalt on hBN and silicon dioxide. It was found that resistivity may was consitstent on hBN and SiO_2 measured as $(0.259 \pm 0.002_{Random} \pm 0.013_{systematic})\mu\Omega m$ and $(0.236 \pm 0.003_{Random} \pm 0.007_{systematic})\mu\Omega m$ respectively, the difference attributed to different growth of cobalt on the two substrates. AMR was found to be 34% higher on SiO_2 compared to on hBN at 0.75% compared to 0.56%. Thermopower was measured to be higher on hBN at $(-39.0 \pm 7.8_{Random} \pm 3.4_{systematic})\mu V/K$ with $(-16.8 \pm 3.3_{Random} \pm 2.1_{systematic})\mu V/K$ measured on SiO_2. The difference here is believed to be due to the effect of hBN on the magnon drag contribution to thermopower. MTEP in cobalt was found to be consistent on the two substrates at (0.18±0.6)% for SiO_2 and (0.13±0.8)% for hBN.

Contents

Introduction

Graphene, first isolated in 2004, and winning the Nobel Prize in 2010, is a single atom thick, hexagonal lattice of Carbon [3]. It is renowned for its record breaking electrical properties and as such is being researched systematically throughout Europe. In a report set out by the European Commission called the Graphene Flagship, the study of Graphene Spintronics was highlighted one of the essential topics of interest. Spintronics is the study of transport of electron spin within a material. Ferromagnetic materials, such as cobalt, have been used to inject (and detect) spin-polarised current into normal metals [4] and recently have been used for spin injection into Graphene. Graphene has the largest recorded spin diffusion lengths, spin lifetimes and highest charge mobility for any known material [5].

Graphene's unique electronic band structure allows spins to travel, unaffected, for record breaking distances, around 10μm at room temperature. Graphene is the only material known to harbour spin lifetimes long enough for practical applications of spintronics thereby enabling the field to prosper. Spin lifetimes have been found to be a factor of 10 larger when Graphene is held on flat hBN as opposed to much rougher silicon dioxide substrates [6]. Encapsulated Graphene heterostructures have been an interesting topic of research recently as they enable the creation of one dimensional edge contacts for probing Graphene's properties [7]. Single layer Graphene is sandwiched between two flakes of hBN, one underneath and one on top of the Graphene. This then exposes the edge of the Graphene at a single point along its edge. cobalt can then be deposited on top of this structure to make electrical contact with just the edge of the Graphene. Hexagonal boron nitride is a substance of particular interest in the field of 2D materials due to its atomically flat crystalline structure and its high thermal conductivity while remaining electrically insulating [8].

cobalt is a material of great interest in thin film research, especially thermoelectric, since cobalt is a ferromagnetic material with a high thermopower [2], [9]. Thin film thermoelectrics is the study of the electricity generated or affected by the presence of a thermal gradient in metallic materials [10]–[12]. Thermoelectrics is a subject of intense research due to its practical, real world applications to energy conservation and reuse. In the future, thermoelectric devices can be attached to or built into electrical devices allow recycling and reuse of waster heat generated. This heat creates a thermalvoltage which can be used to power additional modules in the device, reusing energy and increasing efficiency [12]. In an energy conscious world it is important to increase the efficiency of consumer and industrial electronics to limit reduce the amount of electricity needed to power and reuse them. Exploring and exploiting the properties of new materials, such as Graphene, therefore is a step to creating greener electronics and reducing human impact on the planet and is a key pillar of the Graphene flagship [6].

Currently no published research details how thermal properties of thin cobalt films are affected by being placed on hBN as opposed to SiO_2. Extensive research, however, has been carried out on thermal and electronic transport in cobalt films on SiO_2 substrates [2], [9], [13], [14]. Last semester, a device was fabricated with Electron Beam Lithography techniques to test these properties, full details of measurements and results can be found in last semester's report [15]. Due to complications with the fabrication of the device, here on referred to as "Device 1", no comparisons could be drawn about the difference between cobalt on hBN vs. on SiO_2. Comparing the effect of these two substrates on the cobalt channel therefore was set as the main goal of this semester's research.

Ordered Magnetism

Ferromagnetism and its origin were described in detail in last semester's report, [15], however the main points of interest are summarised below:

- Electrons orbiting a nucleus have an intrinsic, quantised magnetic moment due to their spin and orbital angular momentum and act like little bar magnets

$$\boldsymbol{\mu} = -\mu_B \boldsymbol{L}\,;\ \boldsymbol{\mu} = -g\mu_B \boldsymbol{S}$$

  where μ_B is the Bohr magneton, $\boldsymbol{L}$ is the orbital angular momentum, g is the Lande g factor (2 for electrons[12]) and $\boldsymbol{S}$, the spin angular momentum of an electron [12]

- Magnetisation is a vector field that quantifies n magnetic moments, $\boldsymbol{\mu}_n$ in a given volume, V, and quantifies the macroscopic effect of ferromagnetism (for atoms with net magnetic moments, e.g. cobalt, Nickel and Iron)

$$\boldsymbol{M} = \frac{\sum_n \boldsymbol{\mu}_n}{V}$$

- Magnetic moments can be rotated by an externally applied magnetic field, $\boldsymbol{H}$, that creates a torque, $\boldsymbol{\tau}$, on the moment causing them to align with the field $\boldsymbol{H}$

$$\boldsymbol{\tau} = \boldsymbol{\mu} \times \boldsymbol{H}$$

- Neighbouring spins are governed by the Pauli Exclusion Principle and exchange energy is minimised when neighbouring spins align [16]
- Ferromagnetic materials with shape anisotropy give rise to easy and hard directions of magnetisation $\boldsymbol{M}$
- Shape anisotropy can be exploited in nanodevices allowing easy magnetisation in one direction and hard magnetisation in another thereby allowing effects, such as AMR (see below), to be more easily observed and measured

Understanding these properties was integral to designing a device that could be used to measure properties of a thin ferromagnetic cobalt film.

Anisotropic Magnetoresistance (AMR), also discussed in detail in the previous report, arises in ferromagnetic materials. AMR is a measure of the change in electrical resistance of a material when the angle between the direction of the current flow and the magnetisation direction is altered. Up to a 50% difference in resistance has been measured in certain alloys [17]. The origin of this effect is due to the spin orbit interaction which causes conduction electrons to be scattered at different rates depending on the direction of magnetisation of the material they move in. To quantify AMR, two distinct states are identified arising from rotation of $\boldsymbol{M}$ by an external magnetic field $\boldsymbol{H}$. These two states, defined in terms of resistivity rather than resistance as this is more fundamental, are denoted as $\rho_{||}$ and $\rho_{\perp}$. They relate to the resistivity measured when current flow is parallel and perpendicular to the magnetisation direction. Resistivity as a function of the angle φ between current direction and magnetisation direction is given by the relation:

$$\rho(\varphi) = \rho_{\perp} + (\rho_{||} - \rho_{\perp}) \cos^2 \varphi. \quad (1)$$

A useful figure of merit, along with resistivity, for comparison on hBN vs. SiO_2 is defined as

$$AMR = \frac{\rho_{||} - \rho_{\perp}}{\rho_{||}}\%. \quad (2)$$

Suppression of low energy magnons cause the perpendicular resistivity state to be obscured due to a linear decrease in magnetoresistance at high magnetic field [13]. As such, linear interpolation is required to determine the parallel state, this can be seen in the results sections.

Thermoelectrics

The traditional Seebeck effect, also known as 'longitudinal thermopower', is an effect whereby a potential difference, ΔV, arises in a metal due to the presence of a thermal gradient, ∇T that creates a temperature difference ΔT [12], [18]. Current density, $\boldsymbol{J}$, in a conductor is comprised of two components, one arising from a voltage gradient, ∇V, from Ohm's Law and the other from the thermal gradient ∇T:

$$\boldsymbol{J} = -\sigma \nabla V - \sigma S \nabla T \tag{3}$$

where σ is the electrical conductivity of the metal and S is the Seebeck coefficient. In the steady state case

$$\boldsymbol{J} = \boldsymbol{0} \;\therefore\; \nabla V = -S\nabla T \text{ and experimentally } S = -\frac{\Delta V}{\Delta T} \tag{4}$$

S is positive if there are more positive charge carriers present in the metal and vice versa for negative carriers [12]. Since cobalt has two valence electrons it is negative charge carrier dominant so a negative S is expected to be measured.

A better understanding of thermopower can be gained by imagining the motion of charge carriers within the material. At the hot end of the metal there will be a high occupancy of high energy electron states and a high occupancy of low energy hole states. Conversely, at the cold end there will be a high concentration of low energy electron states and a high concentration of high energy hole states. This causes a diffusion of high energy electrons from the hot end to the cold end and a diffusion of high energy holes from the cold end to the hot end. The reason S can be measured is because of a few differences between electrons and holes in the system

- Scattering rates are different for electrons and holes
- Electrons and holes move at different speeds in the material
- There are different densities of states of electrons and holes at each end

These mechanisms cause there to be a net diffusion of charge which leads to a charge separation and therefore a measureable potential difference.

Following the derivation by Chalmers and MacDonald [12] the conductance can be defined as

$$\sigma = \int -\frac{df(E)}{dE} \cdot c(E) dE \tag{5}$$

where $c(E)$ is the conductivity of the metal as a function of energy and $f(E)$ is the Fermi-Dirac distribution. Thermopower therefore can be written in terms of this conductance as

$$\sigma S = \frac{k_B}{e} \int \frac{E-\mu}{k_B T} \cdot \frac{df(E)}{dE} \cdot c(E) dE \tag{6}$$

with μ as the chemical potential, k_B being the Boltzmann constant, T the temperature of the system and e the elementary charge. By application of a Sommerfeld expansion and the approximation that in metals, charge transport only occurs near the Fermi Level, E_F, it is found that:

$$S = -\frac{\pi^2}{3} \frac{k_B^2 T}{e} \left. \frac{d \ln \sigma}{dE} \right|_{E_F} \tag{7}$$

This expression can then be rewritten in terms of resistivity, ρ, to give:

$$S = -\frac{\pi^2}{3}\frac{k_b^2 T}{e}\frac{1}{\rho(E)}\left[\frac{\partial \rho(E)}{\partial E}\right]_{E=E_F} \quad (8)$$

What is implied here is that thermopower, S, should be affected by the rotation of the magnetisation direction of the Coblat film as S is resistivity dependent [19]. As with resistivity, there are two states, $S_\perp$ and $S_{||}$ that correspond to the perpendicular and parallel orientations of the thermal gradient to the magnetisation direction. The ratio of the difference between these two quantities to the Seebeck coefficient is known as the Magneto-Thermo-Electric Power (MTEP). This quantity will be measured in the cobalt channel on both hBN and on SiO_2.

$$MTEP = \frac{S_{||} - S_\perp}{S_{||}}\%. \quad (9)$$

Design considerations

When designing the new device it was important to keep the contact spacing and dimensions consistent with last semester's device specifications. This was done so that comparisons with last semester's measurements could be made. A full schematic of the contact design can be seen in Figure 2C. Reasoning for the dimensions of given components of the device can be found discussed in large detail in last semester's report [15].

One main aim last semester was to classify the difference in electronic and thermal transport in cobalt on SiO_2 versus on hBN. Due to unforeseen complications in the fabrication process, last semester's device had no working thermometers with which a temperature gradient could be measured. Repairing last semester's device by additional lithographic steps was ruled out early on since the contacts on the hBN were too damaged to fix within a reasonable timeframe and even then a fix was not guaranteed. As such, the design of two new devices was undertaken on two suitably sized, flat hBN flakes, situated on a single SiO_2 wafer. One of these flakes can be seen in Figure 1. Creating two devices increased the chances of obtaining a device that had working thermometers on both hBN and SiO_2. Proximity of the flakes on the SiO_2 allowed for simultaneous lithography and metallic deposition. Contact and channel specification used for last semester's device were duplicated and superimposed on these two new flakes and slightly tailored to fit their individual dimensional constraints. Contact designs were kept as symmetric and uniform as possible.

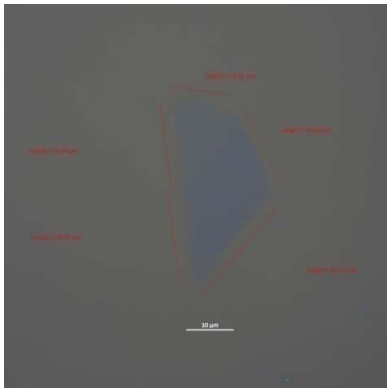

Figure 1: An optical image showing a faint blue flake of hBN of thickness approximately 3nm on a grey background of SiO_2. With a width of order 20μm the flake was large enough to hold both the Cobalt channel and a heater.

Consistent with last semester's device, a channel of thickness 30nm of cobalt with a 2nm gold capping layer, to reduce oxidation, was deposited. On top of this, the contacts were deposited with 100nm of gold and 3nm chromium. It was expected that the contact thicknesses would be 40nm gold and 3nm chromium but an unexpected error during deposition caused more gold to be deposited than expected. Due to this, the fabricated heaters will have a lower resistance than the thin heater last semester so the power dissipated by the heater will be less than that of the previous device. Discussion of how this setback was overcome is detailed in the Measurements section.

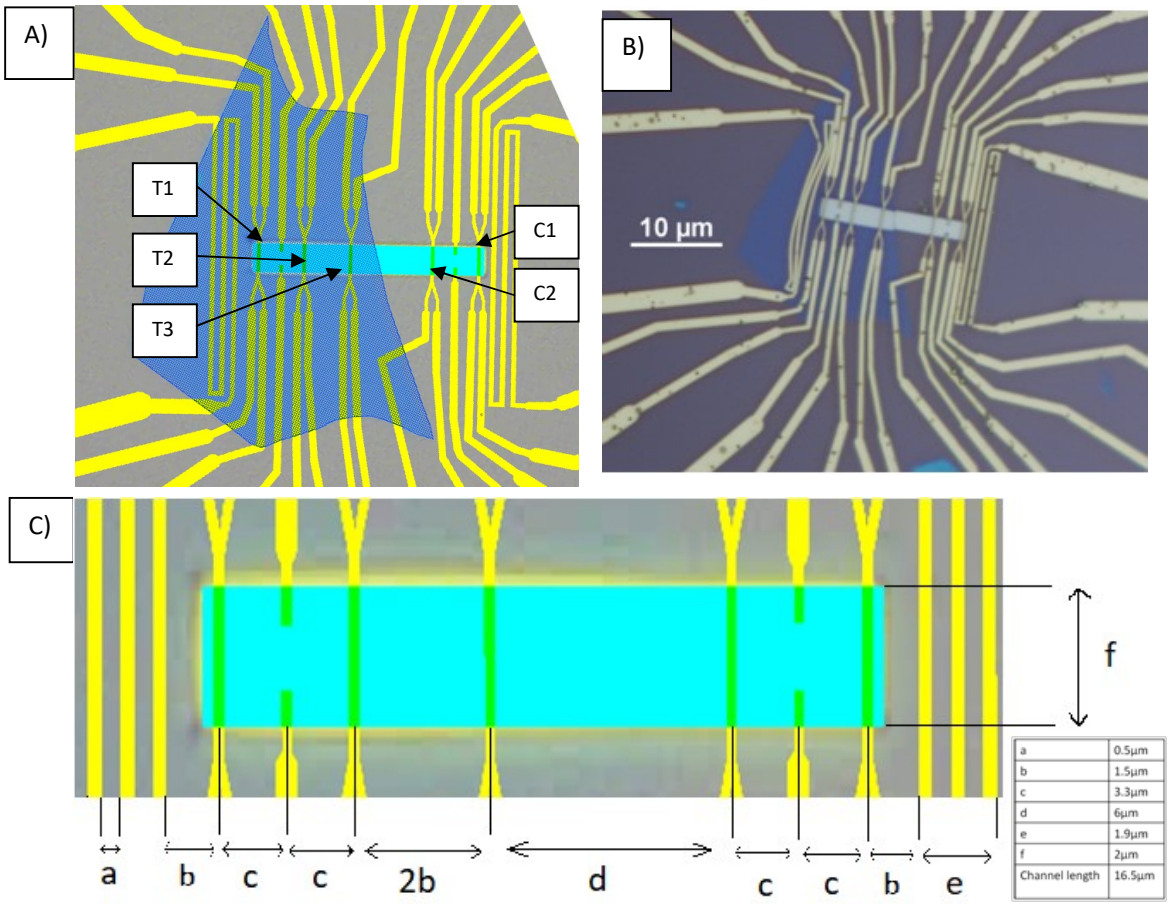

Figure 2. A) Computer generated image of the finalised design sketch for Device 2 drawn up in Layout Editor, ready for lithography. Dark blue represents the hBN flake, bright yellow is Gold (contacts and heaters) and light blue is the cobalt channel. Heater 1 refers to the heater on the SiO_2 and heater 2 is on the hBN flake. B) Device 2 after fabrication and mounting on the LLC. Note the break in the cobalt channel on the edge of the hBN flake. C) A labelled schematic with device dimensions, contact dimensions on the channel are measured from centre to centre. Dimensions are listed in the table to the right.

All thermometers and contacts are 200nm wide and the heaters 300nm wide. Wire width is increased, up to 10µm, as the distance from the cobalt channel increases to increase reliability and, in the case of the heater, reduce nonlocalised heating away from the channel. Thermometers were designed such that a four point measurement (sometimes called "four terminal") technique could be employed, allowing the elimination of lead resistances in measurements. Current is injected and drained along two contacts in a loop and the potential drop is measured across the other two contacts. It is of great importance to employ this four terminal technique as interfacial resistances between electrical contacts and the cobalt channel can vary drastically from contact to contact and from substrate to substrate. This difference arises from chain hydrocarbon molecules of residual PMMA left behind after the first lithographic lift off process (see fabrication section for more detail and context). Gold contacts are deposited onto these residues thus forming a tunnel barrier, greatly affects the resistance between the contact and channel [11]. It is highly preferential to measure the four point resistance of the cobalt channel itself since only cobalt is wished to be classified in these experiments, not the effect of magnetisation of the channel on the interface between contacts and the channel or the contacts themselves. It was shown last semester [15] that the resistance of the gold contacts were not greatly affected (~0.01% variation) by the rotation of the magnetisation of the cobalt channel.

Therefore it is acceptable to assume that any variation in resistance or thermovoltage due to magnetisation direction is attributed wholly to the cobalt channel and not to the gold contacts.

Fabrication

Lithographic process

Fabrication of a device of this kind requires electron beam lithography (EBL). This is necessarily due to the nanometer scale sizes of the contacts only easily achievable with the use of an electron beam. Details of the method of the EBL process can be found in last semester's report [15]but the outline is such. Initially, few layer hBN is isolated by the exfoliation method used by Geim and Novosolov to isolate single layer Graphene [3]. Flakes of hBN are then placed onto a wafer of Silicon which has a 290nm coating of SiO_2 seen in Figure 3 A) the centre, light blue structure being the hBN flake and the darker blue background the SiO_2 coated Si wafer. Next, the process of spin coating is used to cover the sample in a thin layer of PolyMethyle MethAcrylate (PMMA, coloured yellow in B), a material resist that can be weakened under exposure to an electron beam (red). The electron beam is to trace the shape of the cobalt channel as specified seen in C). A solvent is then used to wash away the exposed PMMA area leaving behind a hole in the resist in the shape of the expected cobalt channel seen in D). Deposition of cobalt onto the wafer comes next, shown in grey in E). Finally the residual PMMA and cobalt is washed away with a different solvent leaving behind the cobalt channel atop the hBN flake seen in F). This process was then repeated to deposit the Chromium Gold contacts following which the contacts were then bonded into a chip carrier by a wire bonding machine (not pictured).

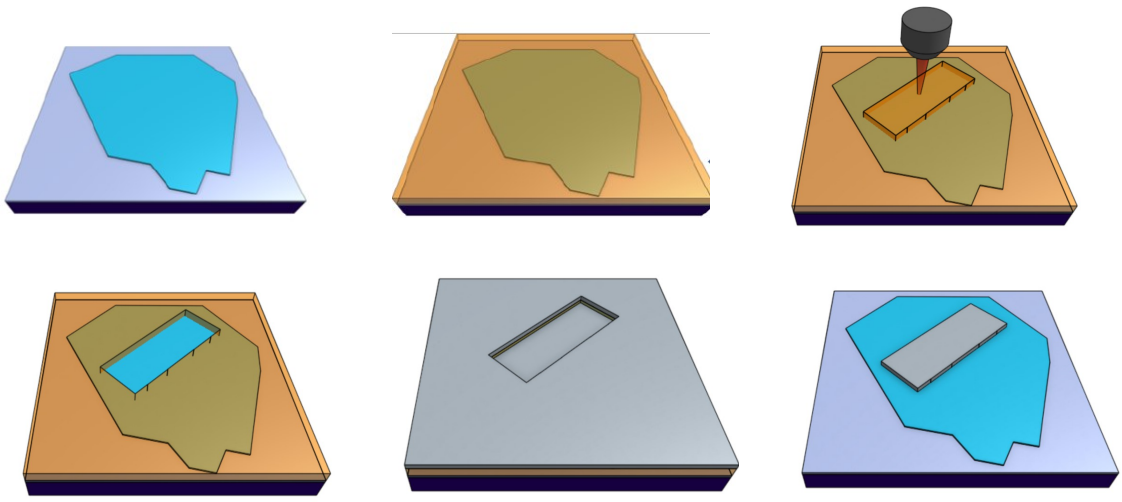

Figure 3: Shown here are the multiple steps taken during Electron Beam Lithography to fabricate the Device 2. A) Flake of hBN exfoliated onto an SiO_2 wafer created by the exfoliation method [3] B) PMMA spin coating of the sample C) electron beam exposure for metallic deposition D) dissolving of exposed region E) metal deposition onto the entire sample F) lift off of the PMMA leaving metallic structure on top of hBN flake. (Images used with permission from Jesus Carlos Toscano Figueroa)

Problems during fabrication

Several major issues occurred during the fabrication of the secondary device that was subsequently not used for measurement, more details can be seen in the Appendix. All three thermometers situated on the hBN were in full working order and the fabricated heater on the Silicon

was in working order. Unfortunately, the heater on the hBN was found to be open circuit and unusable. Due to some small bonding issues no full thermometers on the SiO_2 were fully bonded but two contacts on each thermometer on the SiO_2 were attached. This allows for resistivity/AMR and thermovoltage measurements but no thermopower measurements since no thermal gradient can be measured on the SiO_2 (discussed in the results section). A break in the channel in Device 2 can be seen in FIGURE 2B. This was caused by a combination of the movement of the hBN flake on the SiO_2 substrate due to only being held by Van derWalls forces and the brittleness of the cobalt channel. After mounting and two point resistances checks were conducted it was concluded that there was no electrical contact from any contacts on the SiO_2 to any contacts on hBN. This now limited the thermal transport through the channel. Thermal transport could elicit a thermovoltage in the channel on the hBN via heat transport through the SiO_2 and then hBN substrates but this response would be a reduced thermal response compared to having no break in the channel. In future it would be wise to deposit more Gold on the hBN/SiO_2 transition region to allow for less chance of breaking and a better thermal and electrical continuity across this boundary. It is detailed in the measurements section how noise was reduced and other measurement techniques were employed to measure this low thermal signal.

Measurements

The LLC is mounted in an Oxford Instruments® Microstat HE2 pictured in Figure 4 B. Copper wires connected to the LLC are wrapped around the inside of the Microstat inside of a radiation shield to protect from background radiation that may be present in the lab. These wires are fed out of the Microstat and are connected to a breakout box. The breakout box allows electrical connection to be made to all of device's pins individually. An SRS SR830 DSP Lock-In Amplifier and a Keithley 2602B Sourcemeter can be attached to the breakout box by twist lock connectors, both seen in Figure X. Signals from the device are amplified by a factor of 10 by a SR560 preamplifier to allow a stronger signal to be used for processing in the Lock in Amplifier. A Mercury ITC temperature controller is connected to the Microstat to allow for measurement and regulation of the device's temperature. A turbo vacuum pump connected to the Microstat allowed the device to be kept in a low pressure, 10^{-6} barr, environment to reduce atmospheric contamination. The Microstat was situated in the centre of two large electromagnetic coils that were capable of producing a magnetic field in any in plane direction to the device up to 500mT. Figure 5 shows this experimental setup.

Lead resistances to the device were eliminated by employing a four point measuring technique. Use of a Lock-In Amplifier allowed for precise measurement of potential differences in the system and allowed measurement of second harmonic and out of phase signals key to measuring the Seebeck effect. Details of these two techniques are discussed in more detail in last semester's report. Since all measurements were taken around 300K, thermal fluctuations were present in all measurements. A series of measurement techniques were employed to distinguish desired signals from the high noise in the device. 'Time constant' is a setting on the Lock in amplifier that can be used to change the length of time over which measured A.C. cycles are averaged. A high time constant indicates that a signal measured by the lock in is recorded for a long time, e.g. 30 seconds, and then outputs the average of this signal range therefore reducing the effect of random noise which averages to near zero. Long time constants are used to gain accuracy in measurements that do not change quickly with time. A lower time constant, ~300ms, can be used to look for effects that occur over a short period of time. Many repeat measurements can be taken with low time constant measurements to reduce the random noise through averaging. A combination of how fast the external magnetic field is swept, how high the time constant should be and the number of repeat measurements taken is tailored to each experiment by

conducting trial runs and changing parameters by intuition and familiarity with the lab equipment. Thanks are extended to Christopher Anderson and Jesus Carlos Toscano Figueroa for their kind help familiarising me with the laboratory equipment.

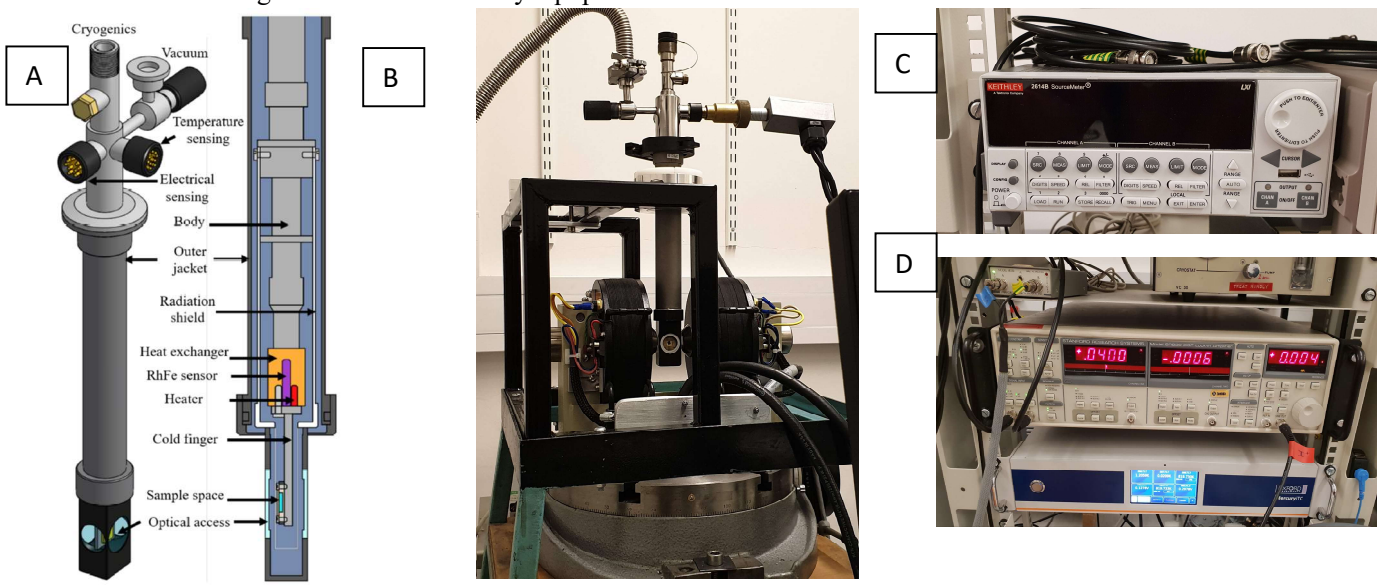

Figure 4: A) Here the LCC sits mounted at the end of the cold finger of a Microstat. A radiation shield helps protect the electronics underneath from external interference. The cold finger allows for the sample to be cooled with cryogenics. The LCC sits in a socket making electrical contact with 24 pin connectors which are attached to an orange ribbon connector. This ribbon leads up the body of the microstat and out of the top via the 'electrical sensing' terminal. This output is seen on the upper right hand side of figure B) as a rectangular box with leads feeding out to a breakout box allowing for direct electrical contact to be made from outside the Microstat to the contacts on the device. B) Here the microstat sits mounted in place aligned vertically between magnetic Helmholtz coils used to apply a transversal magnetic field across the sample. The turbo vacuum pump lead can be seen on the upper left hand side. C) Kiethley variable source meter D) SRS SR830 DSP Lock in amplifier and Mercury ITC temperature controller underneath.

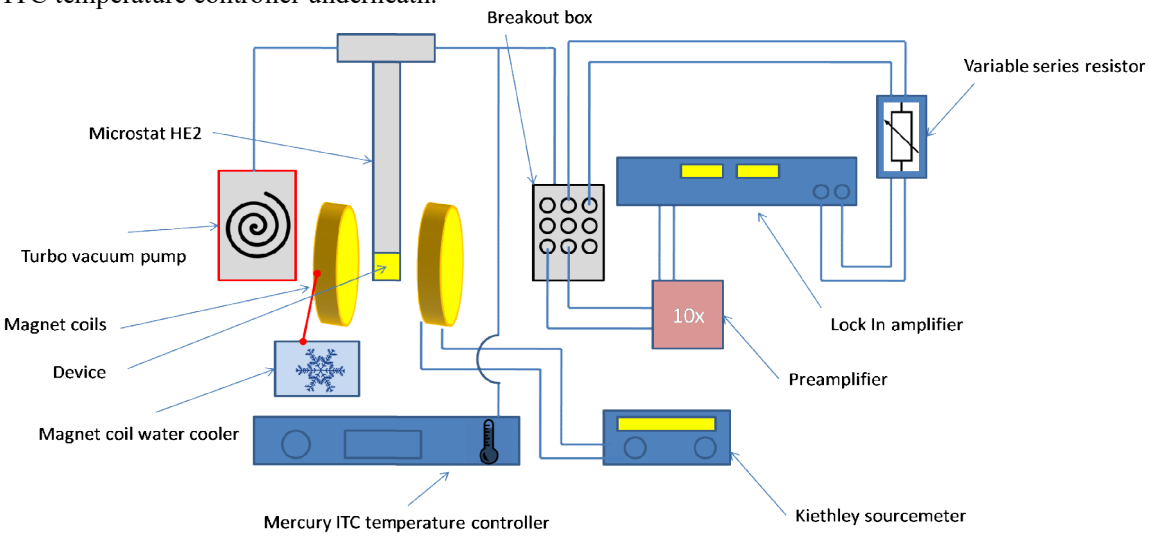

Figure 5: Pictured is an experimental schematic used to illustrate how various components were connected together to perform measurements.

Results

Resistivity and AMR

On SiO_2

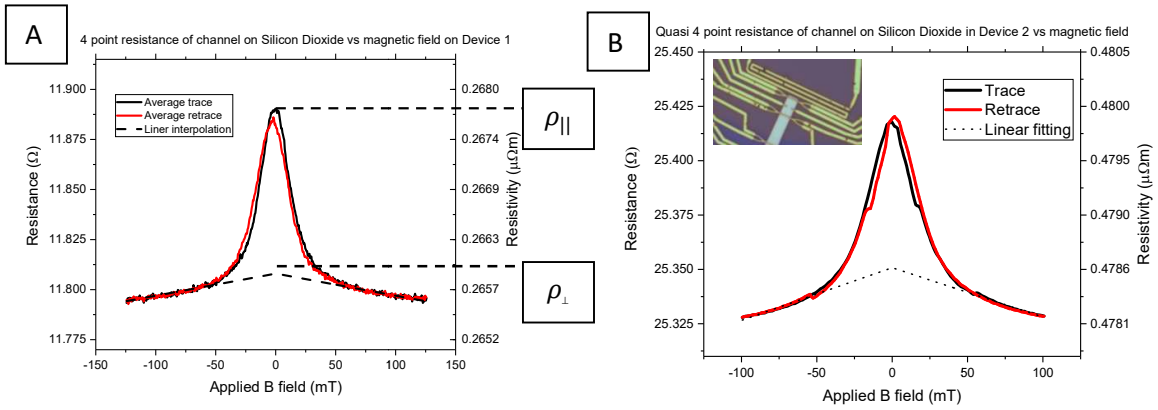

Figure 6: A) Four point resistance of cobalt channel situated on SiO_2 taken last semester B) Quasi four point resistance of cobalt channel on SiO_2 measured this semester.

Resistivity of the cobalt channel last semester was measured to be $(0.236 \pm 0.003_{\text{Random}} \pm 0.007_{\text{systematic}})\mu\Omega\text{m}$ which was found to be consistent with literature sources who tested similar devices [2], [15], [20]. 'Resistivity' here, and in future, refers to the parallel resistivity state, $\rho_{||}$ unless otherwise stated. Details on how this value was calculated from experimental data can be found in the previous report [15]. Resistivity measured from this semester's device on SiO_2 can't be directly compared to literature or last semester's device. A quasi four terminal measuring technique was used to measure cobalt resistance on SiO_2. This implies that the same contacts that were used to measure the potential difference were also used to inject current. As a result, direct comparison between cobalt resistivity on SiO_2 this semester and last semester can't be made. This is due to interfacial and contact resistivities being present in the measurement. With the channel broken across the hBN flake and no hall bars bonded on the SiO_2 region, there are not enough contacts necessary to perform a four terminal measurement. To avoid this problem in the future it would be useful to add another lithographic stage to deposit more gold on the channel break before mounting the device, this would maintain electrical continuity between the two sides of the break.

In Figure 6 A the two states discussed in the Introduction section and in equation 1 can be seen, a parallel resistivity, $\rho_{||}$, and perpendicular resistivity, $\rho_{\perp}$. Linearly decreasing resistance at high field is due to magnon magnetoresistance in which magnons are suppressed by the large applied field [13]. To account for this magnon contribution, a linear interpolation is made and extrapolated to an intersection point at zero applied field to estimate the perpendicular state. Only data points above 50mT and below -50mT were used to construct linear fittings. This establishes consistency between this measurement and subsequent measurements requiring estimation of the perpendicular state. It is therefore assumed that the channel is sufficiently fully magnetised to estimate the perpendicular state when a field above $|50|mT$ is applied.

Change in resistivity due to rotation of channel magnetisation direction due to an external magnetic field can be directly compared between the two devices. Difference between the parallel, $\rho_{||}$, and perpendicular resistivities, $\rho_{\perp}$, is denoted by $\Delta\rho$. It is assumed that the resistivity of the gold contacts and interfacial resistivities are not affected by the direction of magnetisation of the cobalt channel. This can be justified since gold has an AMR response on the order of 0.01%, shown by measurement last semester [15]. Interfacial resistance is predominantly due to PMMA residue left between lithographic stages, separating the channel and contacts. This acts as a weakly magnetic, inhomogeneous tunnel barrier and so it is assumed that its magneto resistive response is negligible [21]. Table 1 summarises the dimensions of the cobalt channel in the measured region and the resistivities, $\Delta\rho$'s and their respective uncertainties. Note, resistivity quoted for Device 2 includes interfacial and contact resistivities so should not be used for any direct comparisons.

Silicon						
	Device 1			Device 2		
Dimensions		% error			% error	
Length	3.14E-06	1.41		3.21E-06	0.75	
Width	2.14E-06	1.59		2.02E-06	2.08	
Thickness	3.31E-08	1.60		3.00E-08	3.10	
Area						
Resistivity	Last semester	% random (fitting)	% systematic	This semester	% random (fitting)	% systematic
ρ⊥ (Ωm)	2.66E-07	1.02	0.27	4.79E-07	0.70	2.69
Δρ	1.77E-09	1.44	0.27	1.30E-09	0.99	2.69
% difference in Δρ	26%					

Table 1: Device 1 refers to the device fabricated and measured last semester and Device 2 this semester's device. "Dimensions", here refers to the dimensions between contacts used for measuring resistivity of the channel.

$\Delta\rho$ in Device 2 is found to be consistent to Device 1 within a 26% range. Mcguire and Potter report, in their comprehensive review of the anisotropic magntoresistance effects in ferromagnetic thin films, that fabrication discrepancies account for large differences in measured $\Delta\rho$ from device to device [22]. They state vacuum quality, deposition rate and even the temperature of the substrate deposited on can affect the measured magnetoresistance of a thin film greatly [23]. Resistivity and AMR of the cobalt channel on SiO_2 last semester agreed with other similarly fabricated thin films of similar thicknesses, [2], [15], [20]. It is found that the $\Delta\rho$ measured in the cobalt channel on SiO_2 is consistent with that of Device 1 so it can be argued that Device 2 is consistent with thin films published in literature. Now comparison between resistivity and AMR on SiO_2 on Device 1 to AMR on hBN on Device 2 can be made as detailed in the next section.

It is interesting to note the slight kink around ±20mT in Figure 6 b). This is due to the cobalt channel being aligned approximately 10^o off from vertical and therefore having a longitudinal component of its magnetisation direction. A switch in the magentisation direction of the cobalt channel is seen at ~5mT in last semester's report under the 'Longitudinally varying magnetic field'[15]. Once the longitudinal component, $Bsin(10^o)$, reaches ~5mT the switch occurs, this happens when B is approximately 20mT as seen in the measurement.

There is a 10% difference between the measured widths of the cobalt channel in Device 2 on hBN vs. on SiO_2. From optical imagery, channel width on hBN was measured to be (2.23±0.04)µm compared to (2.02±0.04)µm measured on SiO_2. This difference arises from the nature of the fabrication process and of the substrate on which electron beam lithography takes place. When the

electron beam is switched on, it causes backscattering of electrons within the substrate. This back scattering causes more PMMA to be weakened, this causes the shape of the hole in the resist to be widened. When cobalt is deposited, the channel will be wider where there is more back scattering. Back scattering is larger on a hBN substrate than on SiO_2 therefore it is expected that the cobalt channel was measured to be wider on hBN than on SiO_2 [24].

On hBN

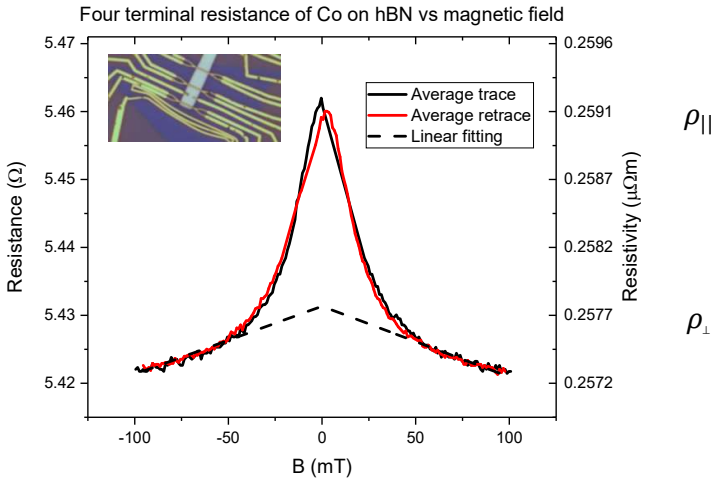

Figure 7: Here the resistance and calculated resistivity of the cobalt channel on hBN are plotted against the applied magnetic field.

Resistivity on hBN of the cobalt channel could be measured directly with a four point technique and was determined to be $(0.259 \pm 0.002_{Random} \pm 0.013_{systematic})\mu\Omega m$. Directly comparing this to the four terminal resistivity of the cobalt on last semester's device, $(0.236 \pm 0.003_{Random} \pm 0.007_{systematic})\mu\Omega m$, shows that the resistivity of cobalt on hBN is greater than it is on SiO_2 by 10%. Since there is a 26% difference from Device 1 to Device 2 (from the $\Delta\rho$ comparison above) it cannot be concluded that the resistivity is necessarily higher on the hBN than on the SiO_2. AFM surface roughness data indicated that the cobalt grew on hBN with more irregularities and less homogeneously than on SiO_2 with surface roughness' having a difference of around 25%. These factors imply that scattering in cobalt on hBN would be larger and therefore a larger resistivity is expected to be measured [24]. This is consistent with measurements taken on the two devices. A four terminal resistance of cobalt on SiO_2 would need to be measured on this semester's device to confirm or deny if the resistivity is indeed higher on hBN vs. on SiO_2. Since there not being enough contacts bonded on the SiO_2 side, this was not possible.

An attempt was made to estimate the four point resistivity of the cobalt on SiO_2 by estimating the interfacial resistances of the three thermometers on the hBN. These resistances were then used to create an average interfacial resistance for contacts. It was then assumed that this average resistance would be the same on hBN and on SiO_2. This average was then subtracted twice, since there are two contacts being used for measurement, from the quasi four terminal resistance measurement on SiO_2. This gave an estimate of the four terminal cobalt channel resistance on SiO_2. It was found that the interfacial resistances varied largely, from 10-40Ω, and that subtracting the average resistance from the SiO_2 measurement yielded a negative resistance for the cobalt on SiO_2. It can be concluded that

interfacial resistances vary too much from contact to contact so no four point resistivity of cobalt on SiO_2 could be determined.

AMR of the cobalt channel measured on hBN was found to be 0.56%. This was measured with a four terminal technique so does not include any additions from the contacts or interfacial resistances. AMR of cobalt on hBN cannot be directly compared with AMR on SiO_2 on Device 2 since AMR depends on the resistivity of the cobalt channel. As a four point resistivity of the cobalt on SiO_2 could not be determined, the AMR therefore will not be accurate. Since continuity between Device 1 and Device 2 has been established it is possible to compare the AMR of cobalt on SiO_2 in Device 1 with the AMR in Device 2 on hBN. Measurements of resistivity, $\Delta\rho$ and AMR are summarised in Table 2. AMR of cobalt on SiO_2 on Device 1 was found to be 34% higher than it is on hBN in Device 2 indicating a weaker magnetoresistive effect of the cobalt on hBN as opposed to SiO_2.

	Device 1	Device 2	Device 2
	SiO2	SiO2	hBN
ρ|| (Ωm)	2.36E-07	4.79E-07	2.59E-07
Δρ	1.77E-09	1.30E-09	1.46E-09
AMR	0.75%	-	0.56%

Table 2: A summary of the resistivities, $\Delta\rho$ and AMR measured of cobalt in both Devices 1 and 2.

Thermal calibration

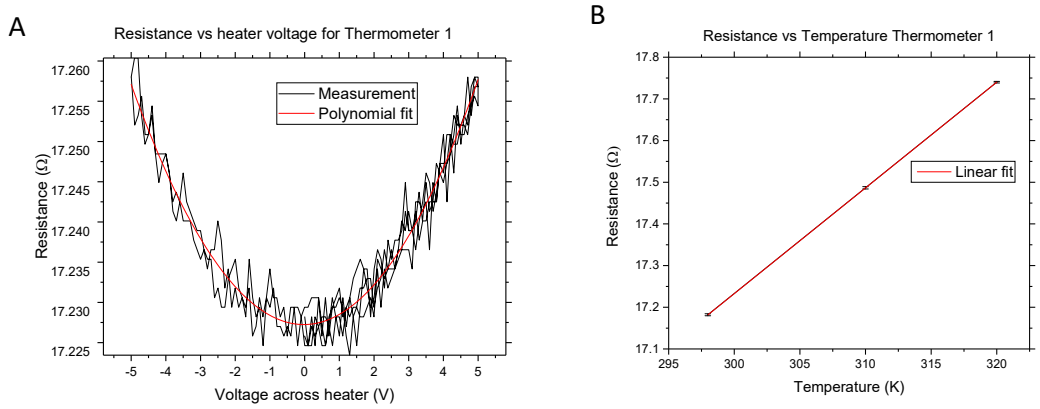

Figure 8. A) Resistance of thermometer 1 for a given potential difference across the heater. B) Resistance of T1 as a response to global temperature increase.

By theoretical work laid out in the 'Thermoelectrics' section it is clear that to find the thermopower of the cobalt, it is necessary to apply a thermal gradient across the channel. It is possible to measure this thermal profile by measuring the four point resistance of the gold contacts on the channel. To do this, the Mercury ITC was used to heat the cold finger within the Microstat, thereby raising the temperature of the device to a known value. Four point thermometer resistances were then measured for approximately 10 minutes and with a 30 second time constant to reduce the effect of background noise and so that an average resistance value could be calculated. This was then repeated for multiple known temperature values the results were plotted in Figure 8A. Resistance was found to be linearly increasing with temperature, which is to be expected [25]. A linear fit yielded a constant of

proportionality, α_i (for a given thermometer i = 1, 2 or 3) with units of ΩK^{-1}, for each thermometer. Next, the Kiethly source meter was used to drive a D.C. current through heater 1 in Figure 2A. This elicits joule heating in the heater therefore creating temperature gradient across the channel. Again, four point resistance of each thermometer was recorded a plot of the voltage across the heater and series resistor vs. thermometer resistance was plotted, see Figure 8B. This response was quadratic in nature, as expected [25], with the coefficient of the voltage squared term being denoted by β_i. A relationship between applied heater voltage and temperature increase of a thermometer, ΔT_i, is now known. The difference in temperature differences between consecutive thermometers, i and j, yields ΔT in equation 4.

$$\Delta T = \Delta T_{Ti} - \Delta T_{Tj} \quad ; \quad \Delta T_{Ti} = \frac{\beta_i}{\alpha_i} V_H \tag{10}$$

Measurement of the potential difference between thermometers while a known heater voltage is applied gives a value for ΔV therefore allowing thermopower, S, to be determined from equation 4.

Thermoelectric measurements

Thermovoltage on SiO_2

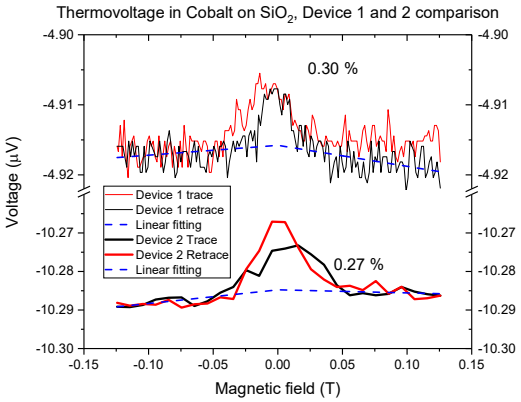

Figure 9 : Thermovoltage measured in the cobalt channel on Devices 1 and 2 due to a thermal gradient imposed by a nanofabricated gold heater vs. applied magnetic field. Device 1 is on top and Device 2 underneath.

Ideally, thermopower would be measured in cobalt on both the SiO_2 and hBN in the same device but there were no fully bonded thermometers on Device 2 on the SiO_2. This meant that no thermometer calibrations could be carried out and so no ΔT could be determined. Last semester, thermopower was measured in cobalt on SiO_2 but not on hBN. Therefore experiments were carried out to compare the thermopower in cobalt on hBN on Device 2 and compare it to the thermopower on SiO_2 in Device 1. In order to compare these two figures, thermoelectric continuity between both devices must be found. To do this, variation in thermovoltage due to the application of an external magnetic field was measured in cobalt on SiO_2 in Device 2 and compared to the same measurement taken on Device 1 on SiO_2.

The exact size of the thermovoltage measurement will not be consistent across the two devices since the temperature gradient created along each of the two channels will differ. In Device 1 the amount of gold deposited to form the contacts was around 40nm compared to over 100nm

deposited in Device 2. Gold films of increasing thickness have a lower resistivity and therefore a lower resistance [26]. Power dissipated two heaters of two different resistances, therefore, will be different since $P = I^2R$. Two point resistance is a measuring technique using the same contacts to inject current and measure potential difference. Along with the two point resistance of the fabricated heaters, the size of the series resistor and the potential difference across the circuit can be used to estimate the power dissipated in each device's heater. A quick calculation shows that the power dissipated in the heater in Device 1 will be approximately half that as in Device 2. See Appendix for details. This is consistent with the measured thermovoltage, around -4.9μV in Device 1 and around -10.3μV in Device 2, approximately double the signal size.

Variation in the thermovoltage signal, *ΔV (not to be confused with Δ,V the voltage created due to ΔT)*, should be consistent between each device since *ΔV* scales with the signal size, *V* [11]. Figure 9 shows both measurements taken with Devices 1 and 2. As with AMR measurements, there are two states used to determine *ΔV*. States are again defined by the magnetisation direction of the cobalt being either parallel or perpendicular to the thermal gradient as discussed in the 'Thermoelectrics' section. Suppression of magnons are present in both measurements as seen by the linear response of the thermovoltage at high magnetic field [13]. Linear fitting and interpolation were again used to determine the parallel state. Consistency was found between the two devices as the ratio of *ΔV* to *V* was (0.30±0.06)% last semester and (0.27±0.03)% this semester for Coblat on SiO_2. Since the devices are consistent, it can be assumed that the thermopower measurements on SiO_2 in last semester's device can be used for comparison with thermopower on hBN this semester.

Identical measurements were taken on the hBN substrate except now, the temperature difference along the channel could be calculated. Use of this temperature difference allows the Seebeck coefficient for cobalt on hBN to be calculated. Figure 11 shows the thermopower measurements of cobalt on hBN in Device 2 compared to thermopower measured in Device 1 on SiO_2. Since heater 2 in Figure 2 was not electrically attached, heater 1 had to be used to provide the temperature gradient in the channel on hBN. Thermal transport in nanostructures is predominantly phonon based, here heat is carried to the cobalt through the SiO_2 substrate and up through the hBN flake, the break in the channel causes a slight reduction in thermal transport from electron transport within the channel [12]. Since the thermometers on the hBN are physically further displaced from the heater than the on the SiO_2 a smaller thermovoltage is expected to be measured in the cobalt on hBN. As distance to the heat source is increase, the rate at which the thermal profile decreases itself decreases as the decay is exponential. This implies that the temperature difference between thermometers far away from the heater will be less than the temperature difference of thermometers closer to the heater. The thermovoltage measured between thermometers will therefore be lower on the hBN than on the SiO_2. Figure 10 best describes this visually.

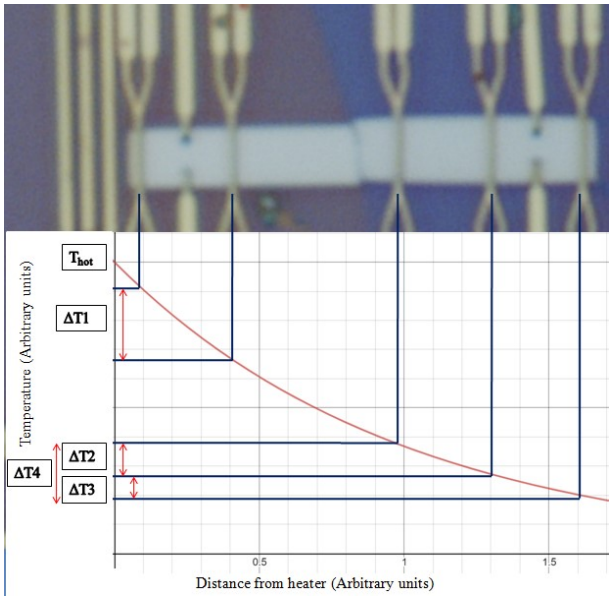

Figure 10: Thermal profile decrease in the channel. It is clear to see that ΔT1 is much larger than either ΔT2 or ΔT3 and so the thermovoltage measured between the first two thermometers will be larger than measured between thermometers 3 and 4 or 4 and 5. ΔT4 however is similar in size to ΔT1 so it will be beneficial to measure the thermovoltage from T3-T1 on the hBN to measure a significant thermoelectric response (as labelled in Figure 2A).

Thermopower on SiO_2 and hBN

Thermoelectric measurements taken on the hBN were measured between T1 and T3 (as labelled in Figure 2A). In addition to this, a series resistor of 500Ω was fabricated to more than double the power dissipated through the heater, (see appendix). This elicits a larger thermoelectric response on the hBN increasing the signal to noise ratio in an attempt to measure ΔV on the hBN. Figure 11 shows the thermoelectric response measured in the cobalt channel on hBN compared to last semester's SiO_2 measurement.

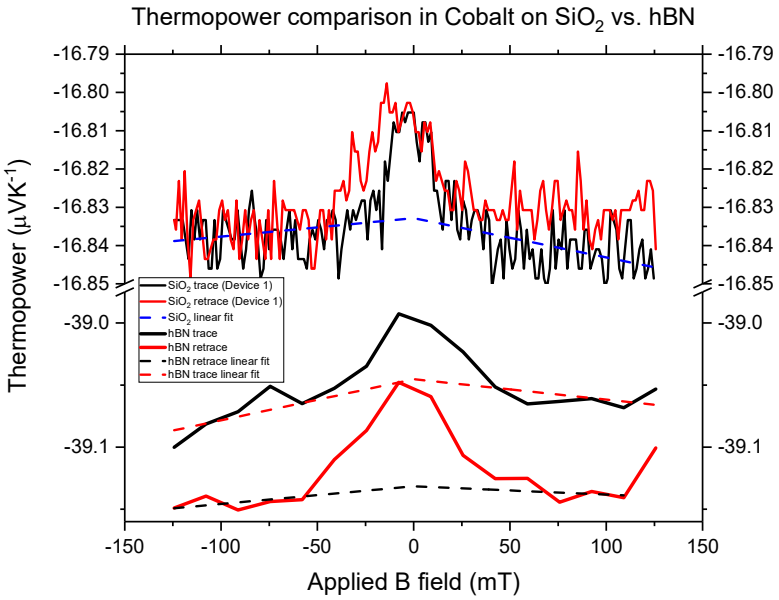

Figure 11: Thermopower measured in cobalt channel on SiO_2 in Device 1 (top curves) and on hBN in Device 2 (bottom curves).

A thermopower signal is measured for Device 2 and it is on the order of μVK^{-1} which is expected for cobalt. Bulk cobalt thermopower is published to be $-25.8\mu VK^{-1}$ [27] but thermopower in thin films tends to be reduced from this bulk value due to size effects. Thermopower measured in cobalt on SiO_2 last semester was found to be $(-16.8 \pm 3.3_{Random} \pm 2.1_{systematic})\mu V/K$ which was found to be consistent with other thin films fabricated in similar ways and also at room temperature [2]. Thermopower is measured to be $(-39.0 \pm 7.8_{Random} \pm 3.4_{systematic})\mu V/K$ on hBN. This is significantly higher than when measured on SiO_2 indicating a strong influence of the hBN substrate on the cobalt's Seebeck coefficient. Equation 8 implies that an increase in resistivity would cause a reduction in thermopower for cobalt on hBN. Resistivity variation from SiO_2 to hBN was around 10% but measured difference in Seebeck coefficient is of the order of 130% indicating that resistivity differences alone cannot describe this difference.

It has been reported that magnon drag is the dominant source of thermopower in cobalt at room temperature [28]. Magnon drag can be thought of by imagining two rough pieces of paper, one stationary on a desk and the other in your hand. Pushing the paper on the desk with the paper in your hand causes the paper on the desk to be dragged along due to the friction between the two sheets. Magnon drag is a similar effect, just replace the paper with magnons and the pushing as a thermal gradient. Magnons are in abundance at the hot end of the channel and diffuse toward the cold end. Along the way magnons drag along charge carriers due to magnon-electron interactions thereby adding to the thermopower of the cobalt channel. Magnon drag is therefore affected by the spin behaviour within the cobalt crystalline structure. It has already been found that cobalt grows differently on the hBN flake than on SiO_2 and so an argument can be made that the hBN is affecting the magnon-electron interaction rate in the cobalt channel thereby increasing the measured Seebeck coefficient.

MTEP from equation 9, can be determined by use of the difference between parallel and perpendicular thermopower states. MTEP on SiO_2 last semester was found to be $(0.18\pm0.6)\%$ and this semester on hBN was found to be $(0.13\pm0.8)\%$. No published literature sources have measured either the MTEP of cobalt on hBN but it has been found that MTEP is consistent with that measured on SiO_2. This indicates a greater thermoelectric response to the rotation of the magnetisation direction on hBN than on SiO_2.

Error estimation

It is impossible to elimintate all errors from a measurement but attemps can be made to reduce their impact and quantify them. Some errors used in calculations are due to limitations of equipment and it is out of the experimenter's control to reduce such an error. An example of this would be the limit of resolution of an optical image of the device. An experimenter can quantify this error by looking at the pixel size relating it to a physical size and ascribing that quantity as the smallest feature an observer can define. Random errors can be reduced by taking repeated measurements of the same experiment and then averaging over these measurements. Error size reduces with the square root of the number of measurements taken [29]. Use of a lock in amplifier increased signal to noise in measurements by reducing the bandwidth of injected and detected current and by the use of filtering. The operating principles of the lock in amplifier are discussed in last semester's report. Table 3 outlines the major contribution to errors within the experiment.

Parameter	Value	Raw error	Percentage error	Source of error
R_S	501.9 Ω	0.1 Ω	0.02 %	Resistance measured with ohmmeter
V_S	5.000 V	0.001 V	0.02 %	Error quoted from the manual of the Lock in amplifier
Cobalt thickness on hBN	33.90 nm	1.50 nm	4.43 %	Thickness from AFM and surface roughness as an estimation of raw error.
Width of cobalt on hBN	2.23µm	0.02µm	1.88 %	Average of three estimations of width along the channel on the hBN flake. Taken from optical imagery with error estimated from pixel size.
Length of cobalt between T1-T2	3.19µm	0.02µm	0.76%	As above.
ΔT	0.076K	0.002K	26.2%	Combination of errors propagated from errors in α and β for each thermometer.

Table 3: Estimation of some of the main sources of error in the experiment.

Propagation of errors was carried out to estimate the error in different derived quantities. Standard error propagation formula were used for simple error estimations [29]. An example for resistivity being:

$$\frac{\delta\rho}{\rho} = \sqrt{\left(\frac{\delta R}{R}\right)^2 + \left(\frac{\delta w}{w}\right)^2 + \left(\frac{\delta t}{t}\right)^2 + \left(\frac{\delta l}{l}\right)^2}\ ;\ \frac{\delta R}{R} = \frac{1}{10}\sqrt{\left(\frac{\delta V}{V}\right)^2 + \left(\frac{\delta V_s}{V_s}\right)^2 + \left(\frac{\delta R_S}{R_s}\right)^2} \qquad (11)$$

This equation was derived from the formula for measured resistivity. V is the measured voltage across the sample, V_s is the source voltage from the lock in amplifier and I is the current assumed to flow through the sample. This current is assumed on the basis that the lock in impedance is much larger than the sample resistance (10MΩ vs. ~10's of Ωs) so the current that flows through the series resistor, with resistance R_s, is the same as the current flows through the sample. The dimensions of the device through which the current flows are t, the thickness, l the length and w the width.

Conclusion

The discovery of Graphene with its record breaking spin properties has enabled the field of spintronics to rapidly advance in recent years [3]. Some of these properties, such as spin diffusion length, are enhanced when Graphene is kept flat on or encapsulated between hexagonal boron nitride substrates [8]. Ferromagnetic materials, such as cobalt, have been used as one dimensional edge contacts to provide less invasive ways of measuring Graphene's properties [7]. Cobalt has also been show to allow the injection and detection of spin polarised current into the Graphene channel. Magneto resistance and thermal gradients can be exploited to alter how these spins are detected and injected [11]. Graphne spintronics is listed by the European Graphene Flagship as a revolutionary new field with the potential for new technological advances such as spin logic gates and more efficient electronic devices [6].

It is therefore important to measure and catalogue the properties of cobalt thin films on hBN substrates and compare their properties to those previously researched on SiO_2. A sophisticated array of equipment including a lock in amplifier and large electromagnet have been used to test the properties of a lithographically fabricated nanodevice. The device consisted of a 30nm thick cobalt channel situated partially on a flake of hBN and partially on SiO_2 with an array of gold contacts that were used to inject current, measure potential differences and measure temperatures along the chanel. Previous experiments with a similar device last semester were unable to draw any conclusions or even comparisons between cobalt on hBN vs SiO_2.

It was found that the resistivity of cobalt on hBN in Device 2 was $(0.259 \pm 0.002_{\text{Random}} \pm 0.013_{\text{systematic}})\mu\Omega\text{m}$, around 10% higher than that measured on SiO_2 in Device 1 $(0.236 \pm 0.003_{\text{Random}} \pm 0.007_{\text{systematic}})\mu\Omega\text{m}$. Resistivity measured last semester was found to be consistent with reported literature for similar thin cobalt films [2], [15], [20]. It is important to note that the variation of resistivity, $\Delta\rho$, due to the rotation of the channel magnetisation from one device to the other show to agree to 26% so it cannot be said for certain that cobalt has a higher resistivity on hBN than on SiO_2. It is expected however that due to the flat nature of hBN, the cobalt grown on top of it will be less dense and will grow more with more discontinuities thereby increasing its resistivity from increased scattering rates [24]. AMR was found to be 34% higher on SiO_2 as opposed to on hBN indicating a weaker magnetoresistive effect due to the hBN flake.

Continuity between thermoelectric measurements between the old and new devices allowed comparison of the thermopowers on SiO_2 and hBN on the two devices. It was found that thermopower was significantly higher on hBN at $(-39.0 \pm 7.8_{\text{Random}} \pm 3.4_{\text{systematic}})\mu\text{V/K}$ compared to $(-16.8 \pm 3.3_{\text{Random}} \pm 2.1_{\text{systematic}})\mu\text{V/K}$ measured on SiO_2. Thermopower on SiO_2 was found to be consistent with published literature for similar thin films [2]. This increase in thermopower cannot be explained solely by the increased resistivity on hBN and by equation 8 as this only accounts for a 10% difference in S. Magnon drag is the dominant source of thermopower in cobalt at room temperature and is dependent on spin transport in ferromagnets. hBN is thought to affect the magnon-electron interaction rate in the cobalt channel due to the different growth of cobalt on hBN. MTEP was found to be (0.18±0.6)% on SiO_2 and (0.13±0.8)% on hBN indicating that the effect of magnetisation direction on the thermopower is larger on hBN than on SiO_2 since thermopower is larger on hBN.

It is recommended that another device be fabricated to attempt to have full working thermometers and four point contacts on both SiO_2 and on hBN. This is technically challenging as the lithographic process is non-trivial and does not have an excellent success rate. Interesting properties are still to be discovered in this area of research. Lower temperature measurements of cobalt on hBN can be used to probe the effect of phonon drag that is predicted to occur at approximately $\theta_D/5$. More complicated effects such as spin transfer torque and much of the field of spin caloritronics are yet to be discovered and more exciting discoveries are bound to be made in this new and hopefully fruitful area of research.

References

[1] L. E. Bell, "Cooling, Heating, Generating Power, and Recovering Waste Heat with Thermoelectric Systems," *Science (80-.).*, vol. 321, no. 5895, p. 1457 LP-1461, Sep. 2008.

[2] A. D. Avery, R. Sultan, D. Bassett, D. Wei, and B. L. Zink, "Thermopower and resistivity in ferromagnetic thin films near room temperature," *Phys. Rev. B - Condens. Matter Mater. Phys.*, vol. 83, no. 10, pp. 1–4, 2011.

[3] K. S. Novoselov and A. K. Geim, "Electric Field Effect in Atomically Thin Carbon Films," *Science (80-.).*, vol. 306, no. October, pp. 666–670, 2004.

[4] M. Johnson and R. H. Silsbee, "Interfacial charge-spin coupling: Injection and detection of spin magnetization in metals," *Phys. Rev. Lett.*, vol. 55, no. 17, pp. 1790–1793, Oct. 1985.

[5] A. C. Ferrari *et al.*, "Science and technology roadmap for graphene{,} related two-dimensional crystals{,} and hybrid systems," *Nanoscale*, vol. 7, no. 11, pp. 4598–4810, 2015.

[6] S. Roche *et al.*, "Graphene spintronics: The European Flagship perspective," *2D Mater.*, vol. 2, no. 3, 2015.

[7] B. Karpiak, A. Dankert, A. W Cummings, S. Power, S. Roche, and S. Dash, "1D ferromagnetic edge contacts to 2D graphene/h-BN heterostructures," *2D Mater.*, vol. 5, p. 14001, 2017.

[8] L. H. Li and Y. Chen, "Atomically Thin Boron Nitride: Unique Properties and Applications," *Adv. Funct. Mater.*, vol. 26, no. 16, pp. 2594–2608, 2016.

[9] T. Böhnert, V. Vega, A. K. Michel, V. M. Prida, and K. Nielsch, "Magneto-thermopower and magnetoresistance of single Co-Ni alloy nanowires," *Appl. Phys. Lett.*, vol. 103, no. 9, pp. 0–5, 2013.

[10] E. Bands, "Nanometer-Scale thermoelectrics," pp. 345–373.

[11] G. E. W. Bauer, "Spin caloritronics," *Spin Curr.*, vol. 11, no. 5, pp. 143–159, 2017.

[12] D. K. C. MacDonald, *Thermoelectricity: An Introduction to the Principles.* New York: Dover Publications, 1962.

[13] W. Gil, D. Görlitz, M. Horisberger, and J. Kötzler, "Magnetoresistance anisotropy of polycrystalline cobalt films: Geometrical-size and domain effects," *Phys. Rev. B - Condens. Matter Mater. Phys.*, vol. 72, no. 13, pp. 1–10, 2005.

[14] T. R. Mcguire and R. I. Potter, "Anisotropic Magnetoresistance in Ferromagnetic 3D Alloys," *IEEE Trans. Magn.*, vol. 11, no. 4, pp. 1018–1038, 1975.

[15] B. Snow, "Magnetotransport in Nanometer thick ferromagnets for Graphene Spintronics," University of Manchester, 2018.

[16] J. G. Soshin Chikazumi, C. D., *Physics of Ferromagnetism*, 2nd ed. Oxford University Press, 2009.

[17] P. Wiśniewski, "Giant anisotropic magnetoresistance and magnetothermopower in cubic 3:4 uranium pnictides," *Appl. Phys. Lett.*, vol. 90, no. 19, p. 192106, 2007.

[18] J. M. Ziman, *Electrons and Phonons: The Theory of Transport Phenomena in Solids*. Oxford: Oxford University Press, 2001.

[19] X. K. Hu *et al.*, "Magnetothermoelectric figure of merit of Co/Cu multilayers," *Appl. Phys.*

Lett., vol. 104, no. 9, 2014.

[20] J. W. C. Devries, "Temperature and thickness dependence of the resistivity of thin polycrystalline aluminium, cobalt, nickel, palladium, silver and gold films," vol. 167, pp. 25–32, 1988.

[21] W. Zheng and S. Wong, "Electrical conductivity and dielectric properties of PMMA / expanded graphite composites," vol. 63, pp. 225–235, 2003.

[22] T. McGuire and R. Potter, "Anisotropic magnetoresistance in ferromagnetic 3d alloys," *IEEE Trans. Magn.*, vol. 11, no. 4, pp. 1018–1038, Jul. 1975.

[23] M. Tokaç *et al.*, "Interfacial contribution to thickness dependent in-plane anisotropic magnetoresistance," *AIP Adv.*, vol. 5, no. 12, p. 127108, 2015.

[24] P. K. J. Wong, M. P. de Jong, L. Leonardus, M. H. Siekman, and W. G. van der Wiel, "Growth mechanism and interface magnetic properties of Co nanostructures on graphite," *Phys. Rev. B*, vol. 84, no. 5, p. 54420, Aug. 2011.

[25] A. S. . Alenitsyn, Alexander G.; Butikov, Eugene I.; Kondraryez, *Concise Handbook of Mathematics and Physics.* CRC Press, 1997.

[26] T. H. Gilani and D. Rabchuk, "Electrical resistivity of gold thin film as a function of film thickness," *Can. J. Phys.*, vol. 96, no. 3, pp. 272–274, 2018.

[27] M. J. Laubitz and T. Matsumura, "Transport Properties of the Ferromagnetic Metals. I. Cobalt," *Can. J. Phys.*, vol. 51, no. 12, pp. 1247–1256, Jun. 1973.

[28] S. J. Watzman *et al.*, "Magnon-drag thermopower and Nernst coefficient in Fe , Co , and Ni," vol. 144407, pp. 1–9, 2016.

[29] G. Kortemeyer, "Error Propagation." [Online]. Available: http://lectureonline.cl.msu.edu/~mmp/labs/error/e2.htm. [Accessed: 01-May-2019].

[30] A. W. Cummings, S. O. Valenzuela, F. Ortmann, and S. Roche, "Graphene spintronics," *2D Mater. Prop. Devices*, vol. 9, no. October, pp. 197–218, 2017.

[31] P. Seneor, B. Dlubak, M. B. Martin, A. Anane, H. Jaffres, and A. Fert, "Spintronics with graphene," *MRS Bull.*, vol. 37, no. 12, pp. 1245–1254, 2012.

[32] A. Hoffmann and S. D. Bader, "Opportunities at the frontiers of spintronics," *Phys. Rev. Appl.*, vol. 4, no. 4, pp. 1–18, 2015.

Health and safety risk assessment

Date:	Assessed by:	Location:
30/09/2018	Ben Snow	Lab room B.008 Schuster building

Task / premises:

Loading and unloading a spintronic device into a microstat and attaching a vacuum pump and other electrical equipment and the associated measurements of such a device. Use of cryogenic liquid helium.

Activity	Hazard	Who might be harmed and how?	Existing measures to control risk	Risk rating
Extended use of computers	Poor working environment	User. Fatigue, stress, muscular or skeletal injury, headaches, eye strain	• Adequate lighting of computer area • No obstructions under desk • Good posture promoting chairs • University support for stress and counselling • Taking frequent breaks and getting fresh air	Medium
Use of electrical laboratory equipment	Electricity, stray wires	User. Electrical shock, burns, fire, tripping over loose wires	• Users are trained and informed how to use equipment before use • All electrical equipment are annually PAT tested and out of date or failed equipment are not to be used • Obvious sparks or damages are reported immediately to lab staff • Grounding bracelets are used when operating electrical equipment • Grounding of electrical equipment • Cable tidy's to keep workspace clear	Medium
Use of pressure valve and lids of liquid helium containers	Dewar exploding	Anyone in the lab	• Pressure must not exceed limit stated on Dewar • Use of safety valve on the dewar that releases excess pressure build up • Specialised connector to dewar that only allows inlet to be connected • Disconnect the decanting line slowly to avoid squirting of liquid helium	Medium
Dispending of cryogenic liquid	Leaks and spills leading to asphyxiation, cold burns from contact with liquid	User and anyone in the lab	• Only those with adequate training are allowed to perform this procedure • Oxygen depletion monitors are kept in the areas near to dewars • Make sure pressure valve is sealed before dispensing liquid • Signs are displayed near liquid helium containers • Cryogenic gloves to be worn to protect from spills • Stand behind the dewar when dispensing takes place • Storage of dewars in well ventilated areas to reduce impact of spillage	Medium

Activity	Hazard	Who might be harmed and how?	Existing measures to control risk	Risk rating
Formation of ice on dewar	Explosion of dewar and ejection of ice at high speed	User and anyone in the lab	• Ice blockages may form inside the dewar neck if moisture comes into contact with the cold gas. This may prevent proper ventilation and unwanted pressure build-up in the dewar • Dewars are fit with protective caps and are checked before use • Never leave dewars uncapped and ensure dewars are empty after use • If an ice plug forms immediately evacuate and alert the School Safety Advisor.	High
Touching cold pipes and surfaces	Cold pipes, exposed cold materials and surfaces	User	• Don't touch cold surfaces and make sure that cryogenic gloves are worn at all times • Burns may take time to manifest after and exposure so call a first aider if there is any doubt about a possible burn	Medium
Breathing in cold fumes and vapour	Mist and fumes from liquid helium	User	• Never consume cryogenic liquid as serious damage can be inflicted to the lungs, mouth and throat. Gas occupies a must greater volume than the liquid so ingesting even a small amount will cause long term, possibly fatal damage	High
Trapping of cryogenic liquid in clothing	Trapped liquid helium in clothing	User	• Always ensure appropriate PPE is worn (cryogenic gloves, aprons etc) • Avoid wearing clothes with pockets or folds that could trap and collect spilt liquid • Never wear shorts or skirts while using cryogenic liquids • Closed toe footwear to be used, absolutely no sandals, flip flops, open toed shoes or shoes not covering up to at least the ankle should be worn • Trousers must fit over top of shoes	Medium
Spillage of cryogenic liquid	Damaged floor and nearby equipment	User and anyone in the lab	• Spilt cryogenic liquid can cause materials and the floor to become brittle and collapse under exposure • Report any spillages to the School Safety advisor immediately and evacuate the building	Low
Use of vacuum pump	Breakage of glass under vacuum	User and anyone in the lab	• Visual check for broken glass before turning on vacuum pump	Low
Use if vacuum pump	Electricity and electric shock	User	• Normal precautions followed when using electrical equipment • Electrical equipment is routinely PAT tested and only equipment that passes these tests are used • Obvious hazards (open wires, sparks etc) are reported to technical staff and removed from the lab	Low
Storing items at height	Objects falling, lifting objects above head height, broken glass or plastic	Anyone in the lab close to the stored items Bodily injuries including cuts or head injuries. Damage to equipment. Contact with harmful substances	• Avoid storing items at height • No storage of hazardous chemicals or substances above head height • No storage of heavy or large items at height • Boxes stored at height must be closed to limit falling of contained items • No glass stored at height	Low

Activity	Hazard	Who might be harmed and how?	Existing measures to control risk	Risk rating
Lone working	No one around to help if an accident occurs or there is an emergency	User	• No lone working allowed in the laboratory under any circumstances	High

Appendix

Fabricated device that was unusable due to broken contacts:

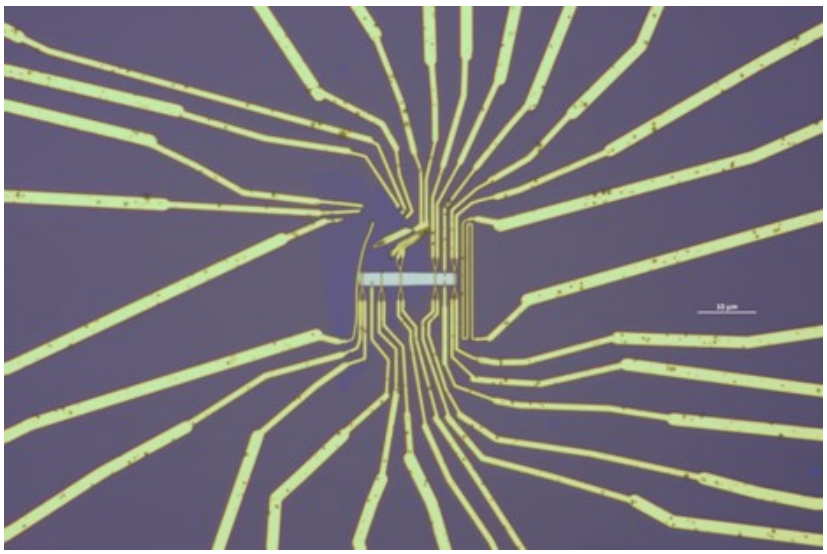

Power dissipation in heater for different devices:

Device 1:
Measured 2pt resistance: 493Ω
Series resistance: 1kΩ
Source voltage: 5V
Current through heater: I = 5/(1000+493)
Power dissipated through heater = I^2R = 0.0055W
Device 2 by same method:
Power = 0.0106
Ratio of power through Device 2 to Device 1 is 1.9